HAL
open science

Multimodality imaging and transcriptomics to phenotype mitral valve dystrophy in a unique knock-in Filamin-A rat model

Constance Delwarde, Claire Toquet, Pascal Aumond, Amir Hossein Kayvanjoo, Adrien Foucal, Benjamin Le Vely, Manon Baudic, Benjamin Lauzier, Stéphanie Blandin, Joëlle Véziers, et al.

To cite this version:

Constance Delwarde, Claire Toquet, Pascal Aumond, Amir Hossein Kayvanjoo, Adrien Foucal, et al.. Multimodality imaging and transcriptomics to phenotype mitral valve dystrophy in a unique knock-in Filamin-A rat model. Cardiovascular Research, 2022, 119 (3), pp.759-771. 10.1093/cvr/cvac136 . hal-03765601

HAL Id: hal-03765601

https://hal.science/hal-03765601v1

Submitted on 20 Sep 2023

HAL is a multi-disciplinary open access archive for the deposit and dissemination of scientific research documents, whether they are published or not. The documents may come from teaching and research institutions in France or abroad, or from public or private research centers.

L'archive ouverte pluridisciplinaire **HAL**, est destinée au dépôt et à la diffusion de documents scientifiques de niveau recherche, publiés ou non, émanant des établissements d'enseignement et de recherche français ou étrangers, des laboratoires publics ou privés.

Multimodality Imaging and Transciptomics to Phenotype Mitral Valve Dystrophy in a Unique KI Filamin-A Rat Model

Constance Delwarde, MSc[1], Claire Toquet, MD, PhD[1], Pascal Aumond, BSc[1], Amir Hossein Kayvanjoo, MSc[2], Adrien Foucal, PhD[1], Benjamin Le Vely, MSc[1], Manon Baudic, MSc[1], Benjamin Lauzier, PhD[1], Stéphanie Blandin, BSc[3], Joëlle Véziers, PhD[4], Perrine Paul-Gilloteaux, PhD [1,3], Simon Lecointe, BSc[1], Estelle Baron, BSc[1], Ilaria Massaiu, PhD[5], Paolo Poggio, PhD[5], Séverine Rémy, PhD[6], Ignacio Anegon, MD[6], Hervé Le Marec, MD, PhD[1], Laurent Monassier, MD, PhD[7], Jean-Jacques Schott, PhD[1], Elvira Mass, PhD[2], Julien Barc, PhD[1], Thierry Le Tourneau, MD, PhD[1], Jean Merot, PhD[1]*, Romain Capoulade, PhD[1]*

[1]Nantes Université, CHU Nantes, CNRS, INSERM, l'institut du thorax, F-44000 Nantes, France
[2]Developmental Biology of the Immune System, Life & Medical Sciences (LIMES) Institute, University of Bonn; 53115 Bonn, Germany
[3]Nantes Université, CHU Nantes, Inserm, CNRS, SFR Santé, Inserm UMS 016, CNRS UAR 3556, F-44000 Nantes, France
[4]INSERM, UMR 1229, RMeS, CHU Nantes PHU4 OTONN, Nantes Univ, Nantes, France
[5]Centro Cardiologico Monzino IRCCS, Milano, Italy
[6]INSERM UMR 1064-CR2TI, Transgenic Rats ImmunoPhenomic, Nantes, France
[7]Laboratoire de Pharmacologie et Toxicologie NeuroCardiovasculaire UR7296, Université de Strasbourg, Strasbourg, France
* senior authors contributed equally

Address for correspondence:
Romain Capoulade, PhD
L'institut du thorax, Inserm U1087/CNRS U6291
IRS-UN, 8 quai Moncousu, BP 70721
44007 Nantes Cedex 1
Email : romain.capoulade@univ-nantes.fr

Or,

Jean Mérot, PhD
L'institut du thorax, Inserm U1087/CNRS U6291
IRS-UN, 8 quai Moncousu, BP 70721
44007 Nantes Cedex 1
Email : jean.merot@univ-nantes.fr

Short title: Pathophysiological Pathways in Mitral Valve Dystrophy

Category: Original Article

Total word count: 8885

ABSTRACT

Aims: Degenerative mitral valve dystrophy (MVD) leading to mitral valve prolapse is the most frequent form of MV disease, and there is currently no pharmacological treatment available. The limited understanding of the pathophysiological mechanisms leading to MVD limits our ability to identify therapeutic targets. This study aimed to reveal the main pathophysiological pathways involved in MVD via the multimodality imaging and transcriptomic analysis of the new and unique Knock-In (KI) rat model for the FlnA-P637Q mutation associated-MVD.

Methods and Results: WT and KI rats were evaluated morphologically, functionally, and histologically between 3-week-old and 3-to-6-month-old based on Doppler echocardiography, 3D micro-computed tomography (microCT), and standard histology. RNA-sequencing and Assay for Transposase-Accessible Chromatin (ATAC-seq) were performed on 3-week-old WT and KI mitral valves and valvular cells, respectively, to highlight the main signaling pathways associated with MVD. Echocardiographic exploration confirmed MV elongation (2.0 ±0.1 mm *versus* 1.8 ±0.1, p=0.001), as well as MV thickening and prolapse in KI animals compared to WT at 3 weeks. 3D MV volume quantified by microCT was significantly increased in KI animals (+58% *versus* WT, p=0.02). Histological analyses revealed a myxomatous remodeling in KI MV characterized by proteoglycans accumulation. A persistent phenotype was observed in adult KI rats. Signaling pathways related to extracellular matrix homeostasis, response to molecular stress, epithelial cell migration, endothelial to mesenchymal transition, chemotaxis and immune cell migration, were identified based on RNA-seq analysis. ATAC-seq analysis points to the critical role of TGF-β and inflammation in the disease.

Conclusion: The KI FlnA-P637Q rat model mimics human myxomatous mitral valve dystrophy, offering a unique opportunity to decipher pathophysiological mechanisms related to this disease. Extracellular matrix organization, epithelial cell migration, response to mechanical stress, and a central contribution of immune cells are highlighted as the main signaling pathways leading to myxomatous mitral valve

dystrophy. Our findings pave the road to decipher underlying molecular mechanisms and the specific role of distinct cell populations in this context.

TRANSLATIONAL PERSPECTIVE

Mechanisms leading to myxomatous mitral valve dystrophy (MVD) remain poorly understood, especially due to the lack of representative models to study this pathology. Thus, we have generated a unique Knock-In rat model for the P637Q mutation on the *FLNA* gene. In the present study, we established the relevance of this model that closely mimicked human disease. The multi-omics approach used revealed multiple pathways with a central role in the pathophysiological processes related to MVD, such as extracellular matrix organization, response to mechanical stress, and an important contribution of immune cells. These data provide mechanistic understandings related to the physiopathology of MV and open new avenues to decipher the underlying molecular mechanisms and identify potential therapeutic targets.

ABBREVIATIONS

AB: alcian blue

AL: anterior leaflet

ATAC-seq: assay for transposase-accessible chromatin

BPM: beat per minute

CCL: cc chemokine ligand

DEG: differentially expressed genes

ECM: extracellular matrix

EF: ejection fraction

EMT: endothelial to mesenchymal transition

FC: fractional shortening

FlnA: Filamin A

GO: gene ontology

GTP: guanosine triphosphate

HPS: hematoxylin phloxin safran

KI: knock-in

MicroCT : micro-computed tomography

MMP: matrix metallo proteinase

MV: mitral valve

MVD: myxomatous valve dystrophy

MVP: mitral valve prolapse

PL: posterior leaflet

PTA: phosphotungstic acid

SEM: standard error to the mean

TGF-β: transforming growth factor β

VEC: valvular endothelial cell

VIC: valvular insterstitial cell

WT: wild type

1. Introduction

Mitral valve (MV) pathologies are a major cause of cardiovascular morbidity and mortality worldwide.[1] Structural MV alterations lead to the development of MV prolapse (MVP), the most frequent form of degenerative MV disease affecting 2 to 3% of the population. MVP is characterized by an excessive systolic displacement of MV leaflets into the atrium associated with an alteration of the layered architecture of the leaflets, including collagen fibers fragmentation and accumulation of extracellular proteoglycans content. Limited by the knowledge of the pathophysiological mechanisms involved in the development and progression of the disease, no pharmacological treatment is currently available to treat MVP, and patients presenting the most severe and symptomatic forms are referred to surgery.[2]

For years, researchers thought that MVP mainly involved a degenerative process linked to aging and a "wear and tear" phenomenon related to the complex mechanical environment, including pulsatile flow, cyclic pressure, bending, and tensile stresses under which MV operates. In the last decade, familial and population genetic screenings have changed this paradigm by identifying genes related to either MVP or myxomatous valve dystrophy (MVD). Our team uncovered the first causal gene associated with MVD by identifying the P637Q mutation in the *FLNA* gene segregating in a large MVD family.[3,4] *FLNA* gene is located in the X-chromosome and encodes for Filamin A (FlnA), an actin cytoskeleton binding protein. Then, the *DCHS1* gene encoding a member of the cadherin superfamily and the cilia gene *DZIP1* were identified.[5,6] Furthermore, additional genetic loci, such as the *TNS1* gene encoding the focal adhesion protein Tensin1, were also associated with MVD.[7–9] Interestingly, all these genes highlight a common pathway related to mechanosensing and stress responses as the main pathophysiological mechanisms involved in the development of MVD/MVP.[10] Thus, studying molecular processes that regulate mechanotransduction arises as the most promising way to determine the underlying processes leading to MVD and opens new avenues to identify potential therapeutic targets. However, there is still a persisting gap linking these genetic mutations to specific and targetable molecular mechanisms.

Our recent works focusing on FlnA-related MVD families revealed a concordant MV phenotype, including classical features of Barlow disease such as the presence of a myxomatous remodeling of the valve with thickened and elongated leaflets, associated with a unique phenotype of restrictive leaflet motion in diastole.[11] At the molecular level, FlnA protein is involved in the response to mechanical stress, interacts with more than a hundred proteins and, thus, plays a role in mechanotransduction, migration, proliferation, morphology, and cell adhesion pathways.[12–15] Using conditional *Flna* Knock-Out (KO) mice developing MVD, we firstly highlighted an interplay between serotonin, transglutaminase 2 and FlnA that regulates the embryonic valve development, as well as activation of Erk signaling in these processes leading to MVD.[16,17] We also showed *in vitro* that *FLNA*-MVD mutations alter the interaction of FlnA with small-GTPase proteins (i.e. RhoA/Rac1 unbalance) and a tyrosine-protein phosphatase (i.e. PTPN12), modifying the F-actin network and, therefore, the stress response.[18,19] We have recently confirmed these results *in silico*.[18–20] Together these findings suggest that MVD-associated FlnA mutations are loss of function mutations. However, they remain limited by the lack of representative models with endogenous expression of mutated proteins. To overpass these limitations, we generated a unique rat model Knock-In (KI) for the FlnA-P637Q mutation.[21]

The current study aimed to phenotype our novel KI rat model developing mitral valve dystrophy (MVD) and, thereby, constituting a valuable model to decipher the MVD-associated pathophysiological pathways. We established the relevance of our model that closely mimicked the disease observed in patients and performed a transcriptomic analysis. We revealed the involved signaling pathways, such as extracellular matrix organization, epithelial cell migration, and molecular stress, as hypothesized based on our previous works. Additionally, we identified a central contribution of immune cells in the pathological process leading to MVD.

2. Methods

Detailed procedures and protocols are provided in the Online Supplementary Material.

2.1 Rats

Sprague-Dawley FlnA-P637Q Knock-In (KI) rats were engineered using Crispr/Cas9 methods and founders were characterized at the Transgenic Rats and ImmunoPhenomic (TRIP) facility in Nantes (France).[21,22] All the analyses between KI and Wild-Type (WT) were performed on littermates.

2.2 Mitral valve phenotyping

Multimodal and complementary imaging approaches were used to phenotype the MV of 3-week-old and 3-to-6-month-old rats. 2D Doppler-echocardiography was used to assess MV morphology and function, micro-computed tomography (microCT) provided a 3D quantification of the MV volume, and standard histological stainings the composition and remodeling of the leaflets' extracellular matrix (ECM). Anterior and posterior MV leaflets were also separately analyzed.

2.3 RNA-sequencing data generation and bioinformatic analysis

5 WT and 5 KI mitral valve leaflets (i.e. anterior + posterior) from 3-week-old rats were harvested for RNA-seq analysis. After RNA extraction (Qiagen miRNeasy micro kit) and quantification, the library was generated *via* SmartSeq 2 (SS2). For statistical analysis, the raw read counts were imported into DESeq2 (v. 1.30.1) using R (v. 4.0.4).[23] To identify the differentially expressed genes (DEGs) of particular interest to the development of mitral valve dystrophy, we selected genes with a p-value <0.05 and Fold Change (FC) >1.2 or FC <0.8. Enrichment analysis was done on these genes using clusterProfiler package (v. 4.0.0).[24] Significant GO-terms (p<0.05) parts of similar pathways were grouped under 3 metaclusters (MC) (i.e. hypothesis-free analysis). We finally designed specific MCs that encompass pathways described in the literature as involved in the MVD (i.e. hypothesis-driven analysis).

2.4 qPCR data generation to assess anterior versus posterior MV leaflet transciptomics

RNA extraction was performed separately on anterior and posterior MV leaflets from 12 WT and 12 KI 3-week-old rats using the miRNeasy mini kit (Qiagen). Reverse transcription was done using the High capacity cDNA reverse transcription kit (Applied Biosystem). The qPCR reaction was performed using the Power SYBR green PCR master mix (Applied Biosystems), targeting *Gapdh*, *Has1*, *Esm1*, *Cspg4*, and *Ccl7* genes (Table S1; Online Supplementary Material). A comparison of relative expression was conducted between genotype, and leaflet (i.e. anterior *versus* posterior).

2.5 Assay for Transposase-Accessible Chromatin (ATAC)-sequencing and computing analysis

We performed an open chromatin assay for transposase-accessible chromatin using sequencing (ATAC-seq) to detect differences in active profile in chromatin between 3 samples (50 000 cells/samples; pool of MV from 8 animals/sample) of 3-week-old WT and KI rats. Differentially opened regions between the KI and WT conditions were selected based on a log2 fold change of 1 and FDR of 10% using edgeR quantile-adjusted conditional maximum likelihood (qCML) analysis.[25] Motif enrichment analysis was performed using MEME-Chip, using all called peaks between conditions as a background.

2.6 Statistical analysis

Data are expressed as means ± standard deviation (SD) or median (IQR), as appropriate. Images presented throughout the manuscript are representative of analyzed samples for each genotype. Non-parametric Mann-Whitney test or Wilcoxon test were used as appropriate.

Data were analyzed using GraphPrism software, v8. A p-value <0.05 was considered significant.

2.7 Study approval

All rat experiments were carried out following European Union Directive 2010/63/EU about the protection of animals used for scientific purposes and were authorized by the French Ministry of Higher Education and Research after approval by the Ethics Committee on Animal Experimentation from the Région Pays de la Loire (approval numbers: APAFIS 6687 & 33433).

Animals were housed in a controlled environment (under a 12h light/dark cycle with ad libitum access to food and water) in the specific pathogen-free animal facilities at the Unité Therapeutique Expérimentale in Nantes (France), an animal care facility endorsed by French Ministry.

3. Results

3.1 Transgenic KI FlnA-P637Q rat model: breeding and anthropometric data

The proportion of genotypes of male and female rats coming from either heterozygous ♀ $^{+/-}$ x KI ♂ $^{-/-}$ (n=59 matings) or heterozygous ♀ $^{+/-}$ x WT ♂ $^{+/+}$ (n=45 matings) crossings follow a Mendelian genetic scheme according to *FLNA* gene location on the X chromosome (Figure S1A; Online Supplementary Material). The anthropometric data at the weaning (3-week-old) were recorded in male WT (n=5-6) and KI rats (n=11-12): body weight and tibial length were similar in both genotypes (Figure S1B & S1C; Online Supplementary Material). No difference in terms of anthropometric data was also observed between WT and KI in females and in adult rats from 3-to-6-month old (all p>0.05).

3.2 Mitral valve phenotype in the 3-week-old KI rats

Based on the morphological and functional echocardiographic evaluation of the MV apparatus, blinded for genotype, the genotype/phenotype correlation turned out to be fully concordant: all animals classified with MVD were KI. Although MV regurgitation was not detected in these 3-week-old rats, the restrictive leaflet motion in diastole specifically reported in FlnA families, as well as leaflet prolapse, were observed in KI rats (Figure 1A and 1B). Moreover, KI rats had a longer anterior MV leaflet compared to WT (2.0 ±0.1 mm *versus* 1.8 ±0.1 mm, p=0.001; Figure 1C), and a trend for larger annulus diameter in KI animals (2.3 ±0.17 mm *versus* 2.1 ±0.12 mm; p=0.06; Figure 1D). Overall, Doppler-echocardiographic examinations of the MV apparatus, that were performed on the same hemodynamic environment (i.e. equivalent heart rate in KI versus WT animal; Figure 1E), support the presence of a MV dystrophy in the transgenic rat model mimicking the phenotype observed in *FLNA* mutated patients. The indices of LV morphology and function were similar in KI and WT 3-week-old rats (Table S2, Online Supplementary Material).

To overpass the potential bias related to the 2D assessment of a 3D structure such as the MV and the heterogeneous expression of the MV dystrophy over each leaflet, we developed an innovative

approach based on microCT to quantify the volume of each MV leaflets. Following manual segmentation and semi-automated thresholding, we showed that KI rats had significantly higher MV volume than WT littermates (+58%; p=0.02; Figure 2G). Noteworthy, there was no difference between the increase of anterior *versus* posterior MV leaflet volume in KI rats (+66% *vs* +71%, respectively; p>0.90; Figure S2, Online Supplementary Material). These data confirm the presence of a dystrophic MV, affecting both leaflets, in transgenic rats and highlight the heterogeneous nature of the remodeling along the leaflets, mostly observed in the distal sections (Figure 2H).

We performed a qualitative and quantitative analysis of the macroscopic and microscopic features of MV from KI (n=10) and WT (n=5) animals (Figure 3). Macroscopically, anterior and posterior MV leaflets from WT rats were translucent as compared to KI rats, in which MV tissue appeared white and opaque (Figure 3A). Of note, the subvalvular apparatus was significantly remodeled with fewer but thicker chordae tendinae in KI animals compared to WT (15 ±4 *versus* 24 ±4; p<0.0001; Figure 3A,A'). Histological analysis of the anterior and posterior MV leaflets of 3-week-old WT rats showed thin and well-organized leaflets: the fibrosa layer was continuous all along the leaflet, displaying a dense collagen strip (Figure 3B, D, H, and L). According to the light alcian blue staining, the ECM was poorly charged with mucopolysaccharides (Figure 3C and J). Overall, the leaflets were mostly covered by flat endothelial cells (Figure 3H) and exhibited minimal free edge enlargement (Figure 3B). As opposed, KI animals presented thickened and mucopolysaccharides-rich MVs, supporting the myxomatous remodeling of their ECM (Figure 3E, F, G, I, K, and M). No sign of calcification was detected in either WT or KI animal MV (negative Alizarin Red staining; data not shown).

Histological abnormalities were observed in 9 out of 10 KI rats. Among these 9 rats, 6 (66%) had both leaflets affected, 1 had only the anterior leaflet affected while the 2 others exhibited remodeled posterior leaflet only. In 50% of the KI rats, thickening and diffuse disorganization were mostly observed in the distal two-thirds of the leaflets (Figure 3E-G), whereas heterogeneous remodeling was observed in the other half of the KI rats. Only 2 KI rats exhibited a well-defined and collagen-rich fibrosa

layer. Compared to the WT, KI MVs appeared immature and displayed mucopolysaccharides enrichment (hyaluronan, glycosaminoglycan) (Figure 3F, K) with very little collagens (Figure 3G, M). Noteworthy, in most of the cases, KI leaflets presented swollen endothelial cells compared to WT (Figure 3I). In addition, two cases presented a focal remodeling (Figure S3; Online Supplementary Material)

We developed a histological-related image processing approach to quantify MV remodeling. This analysis confirmed the global thickening of both the anterior and posterior MV leaflets (MV thickness: +53% p=0.002) coupled with enrichment of mucopolysaccharides (Alcian Blue signal: +217%; p=0.027) in KI animals compared to WT. Furthermore, the quantitative analysis highlighted the regionalized nature of the remodeling along the leaflets. We quantified a 4-fold and 2-fold increase of their thickness in the second and last thirds of the leaflets (p=0.002 and p=0.049, respectively; Figure 3N) whereas the content in mucopolysaccharides was persistently increased in KI MVs by 4-fold in these distal sections (p=0.037 and p=0.027, respectively; Figure 3O).

Importantly, homozygous 3-week-old female KI rats exhibited myxomatous MV dystrophy with similar features as those observed and quantified in males (Figure S4 A,B; Online Supplementary Material).

Overall, all these phenotypic data, from the functional to the macroscopic tissue analysis, confirmed that the KI rat model for the FlnA-P637Q mutation exhibits a myxomatous MV dystrophy, as early as 3-week-old, and is thus a pertinent model opening new avenues to study pathophysiological mechanisms related to MVD.

3.3 Evolution of mitral valve dystrophy in adult KI rats

To analyze the evolution of MVD with aging, quantitative echocardiographic, microCT and histological analyses were performed on 3-to-6-month-old rats. These studies revealed that the increase of the anterior leaflet length and width measured by echocardiography, as well as the increase in MV volume (microCT), were retained in KI adult rats as compared to WT littermates (all p<0.05; Figure S5 A-C; Online Supplementary Material). As opposed to the WT adult rats where MV regurgitation was never

recorded, we observed minimal MV regurgitation in KI animals (i.e ≤mild regurgitation) that did not yet determine myocardial remodeling or dysfunction (Table S2; Online Supplementary Material).

Histological analysis at later stages confirmed the presence of a myxomatous MV remodeling in adult KI rats with similar features, in both anterior and posterior leaflets, as observed in 3-week-old animals (Figure S5D; Online Supplementary Material).

These data on the evolution of the MV dystrophy in adult KI rats emphasized the persistence of the phenotype and then strengthen the pertinence of the FlnA-P637Q KI rat model to decipher pathophysiological mechanisms leading to this frequent human disease.

3.4 Molecular phenotyping to identify the signaling pathways related to mitral valve dystrophy.

To determine the pathogenic mechanisms that contribute to the MV remodeling in the 3-week-old KI rats, the transcriptome of pooled anterior plus posterior MV leaflets has been analyzed by RNA-sequencing. After quality control, 4 KI and 5 WT samples were compared. 15102 gene transcripts were identified and aligned. RNA-seq analysis of the 524 gene transcripts differentially expressed between WT and KI animals ($p<0.05$) revealed that they clearly segregate in up (FC >1.2) and down-regulated (FC <0.8) gene clusters (257 and 268 transcripts, respectively) (Figure 4A).

The enrichment of these DEGs in GO-terms and GO-terms metaclusters (MCs) created on both hypothesis-free (MC1-3) and hypothesis-driven analyses (MC4, 5) are presented in Figure 4B. The GO-term analysis identified one major pathway related to chemotaxis and immune cell migration that encompassed 30% of the significant GO-terms (10/34 GO-terms): the first metacluster (MC1), called "chemotaxis and immune cell migration", was built accordingly. The two most significant GO-terms in the MC1 were "cell chemotaxis" and "leukocyte migration" (GO:0060326, $p=2.31x10^{-5}$ and GO:0050900, $p=3.77x10^{-8}$; respectively). Upregulated genes from MC1 included chemokines *Ccl28*, *Ccl7*, pro-inflammatory proteins *S100a8* and *S100a9, Il16, Itgax, Itga9,* or endothelial cell adhesion molecule *Madcam1* (all $p <0.05$; Table). The second family of significant GO-terms was related to the extracellular matrix and grouped under the MC2, "extracellular matrix". The most significant GO term

in the MC2 was “extracellular matrix organization” (GO:0030198, $p=9.85x10^{-6}$). Genes coding for metalloproteinases (*Mmp12*, *Mmp17, Adamts7*) and hyaluronic acid synthase (*Has1)* were upregulated in the KI condition compared to WT (Table). The GO-term “epithelial cell migration” (GO:0010631,$p=1.47x10^{-5}$) was found in this unbiased analysis together with the “epithelium migration” GO-term, two GO-terms used to create the MC3 “epithelial cell migration”. Genes such as *Klf4*, *a*nd *Hbegf* were upregulated in KI compared to WT animals (Table).

Because endothelial to mesenchymal transition (EMT) has been described in the literature as a potential contributor to the development of MVD,[10,26] we built the MC4 related to “endothelial to mesenchymal transition”. In this hypothesis-driven analysis, KI and WT samples consistently clustered, and the association was driven by genes such as *Wnt2* and *Tmem100* (Table). Similarly, to test the implication of molecular stress pathways, we built the MC5 comprising mechanotransduction-related GO-terms: genes such as *Bmp7*, proteoglycan *Cspg4*, secreted glycoprotein *Slit2*, the mediator of TGF-β transduction *Smad4,* BMP-antagonist *Grem1* were found upregulated in this second hypothesis-driven analysis (Figure 4B; Table).

The sensitivity analysis confirmed the involvement of these pathways, grouped under MCs, in the development of MVD (Figure S6; Online Supplementary Material). The complete list of genes in each MC is included in the Online Supplementary Material (Table S3).

qPCR experiments confirmed the upregulated expression of key genes in KI compared to WT MV (i.e *Has1*, *Esm1*, *Cspg4*, and *Ccl7*; Figure S7, Online Supplemental Material). Furthermore and concordant with the comparable phenotypic remodeling observed in the anterior and posterior MV leaflets, similar increases in the expression levels of these genes were detected in both leaflets (Figure S7; Online Supplementary Material).

3.5 Regulome remodeling in mitral valve dystrophy

Next, using ATAC-seq, we analyzed the differential chromatin opening between MV cells from KI and WT rats to uncover key transcription factors (TF) driving MVD and potentially those that account for

the differential gene expression patterns we highlighted. After quality control, 2 KI and 2 WT samples were analyzed. 373 differently opened regions were identified between KI and WT conditions. Gene proxy annotation of these 373 regions highlighted an enrichment for the "Wnt signaling" (Wikipathway 2021) and the "acting binding" (GO molecular function) pathways, that were not statistically significant after adjustment (data not shown).

Whole genome foot-printing analysis revealed a differential TF binding dynamic for 21 TFs on the chromatins of KI and WT cells. As illustrated on the volcano plot and the aggregated imprint of FOSL1 and JUND in Figure 5A, 17 TFs exhibited higher chromatin binding signal in KI valvular cells compared to WT (BACH1, BACH2, BATF, ETV6, FOSB, FOS, FOSL1, FOSL2, JDP2, JUN, JUNB, JUND, MAF, MAFK, NFE2, NFE2L2 and SPI1). On the other hand, E2F4, HINFP, NRF1, TFDP1 revealed lower binding dynamics in KI cells' chromatin (Figure 5A and supplementary Table S3). Enrichment analyses for these TFs with differential binding imprint, using the Panther and Wikipathway databases, pointed to the TGF-β signaling pathway (adjusted p-value: 3×10^{-5} and 6.5×10^{-9}, respectively; Figure 5B), known to be involved in MVD development. Additionally, the significant association for inflammation and interleukin pathways in Panther (adjusted p-value: 7.2×10^{-3} and 1×10^{-2} respectively) and hematopoietic stem cell differentiation pathways in Wikipathway (adjusted p-value: 7.6×10^{-6}) are in line with molecular mechanisms and signaling pathways highlighted by our RNA-seq analysis as involved in the development of MVD.

Interestingly, differential chromatin opening was observed in the loci of DEGs identified in RNA-seq analysis. As illustrated in Figure 5C, *Cspg4* and C*ilp* exhibit differentially opened binding site for the TF ETV6 in KI compared to WT. A differentially open binding site for FOSL2 in *Wnt2* gene locus was also identified. *Cep83* gene also exhibited differential chromatin opening (Figure 5C).

4. Discussion

This study reports the first rat animal model of myxomatous mitral valve dystrophy observed in MVP patients; the FlnA-P637Q KI rat. The molecular analyses performed on the MV validate stated hypotheses and open new ones regarding pathophysiological mechanisms involved in the disease. Indeed, we confirm that ECM regulation and mechanotransduction play a central role in the process leading to MVD. Our findings also pointed out the activation of EMT and epithelial cell migration in the disease and the central role of immune cells in MVD.

4.1 The FlnA-P637Q KI rat as a new and unique model to study mitral valve dystrophy

Relevant animal models are essential to unravel the pathophysiological mechanisms leading to complex diseases, such as MVD. Although small-breed dogs and rodent-based KO animal models offer important benefits to decipher the molecular mechanisms leading to MVD, considerable limitations restrain their usefulness.[16,17,27,28]

To overpass these limitations and improve our ability to image the MV, we have created the FlnA-P637Q KI rat, a model which also appears to better mimic several human diseases than mouse model.[29] Our findings show that the FlnA-P637Q rat develops MVD with a myxomatous feature by 3 weeks of age. Interestingly, the phenotypic data we reported are consistent with clinical data described by our team in patients with FlnA-MVP mutations.[11] Indeed, we observed an elongation and thickening of MV leaflets with the presence of a billowing/prolapse. Furthermore, rat MV leaflets also exhibited the typical restrictive motion in diastole as well as some dystrophic features on the subvalvular apparatus. Thanks to the development of a new and innovative microCT approach we quantified a 58% increase in FlnA-P637Q MV leaflets volume compared to controls which is in agreement with the 53% increased thickness quantified by histological analysis of the 3-week-old KI animals. Noteworthy, both anterior and posterior MV leaflets, in males and females, were remodeled and displayed similar regionalized ECM disorganization with an accumulation of proteoglycans in their distal two-thirds.[30,31] In adult rats, valve dystrophy persisted and presented similar structural remodeling as observed in juvenile rats and

human MVD. At this later stage, we also reported the presence of mild regurgitation in KI animals (i.e. regurgitation without significant hemodynamic consequence for the heart) that did not translate to LV remodeling and function impairment. Nonetheless, we reported significant alterations of the subvalvular apparatus, with thicker chordae and less chordae branching, that in turn could lead to the modification of applied forces on the MV and thus modulate the underlying pathophysiological mechanisms leading to MVD. Indeed, recent evidences pointed out the remarkable ability of the MV to adapt to the changes in mechanical and hemodynamic conditions, especially in the context of ischemic MV disease related to LV remodeling.[32,33]

In the present model, MV thickening and elongation could not be related to LV dilatation nor papillary muscle displacement. These data emphasize the recognized evolutive nature of MVD and suggest LV remodeling is not yet engaged at this adult stage. Future studies are needed to clarify this point and investigate the evolution and consequences of the morphologically and functionally impaired MV on older and/or heamodynamically challenged animals, which would be concordant with the increased incidence of significant MVD/MVP with aging in human.[1]

Together, our observations validated the relevance of the FlnA-P637Q KI rat to model MVD and to study the pathophysiological mechanisms leading to the disease.

4.2 Extracellular Matrix, Molecular stress pathways, Epithelial cell migration, EMT and Chemotaxis and immune cell recruitment are associated with mitral valve dystrophy

Despite the high frequency of MVD, there is still a lack of knowledge concerning the mechanisms associated with the disease. Consistent with genetic findings on MVD, we identified ECM homeostasis (i.e. MC2 “Extracellular matrix”), response to mechanical stress (i.e. MC5 “Molecular stress pathways”), and Wnt and TGF-β molecular signatures in FlnA-MVD rats.[4–8] These findings are concordant with the observed myxomatous ECM remodeling in the KI mitral valves and the well-recognized role of FlnA as a scaffolding network protein, a sensor and a regulator of cellular response to mechanical stress.[12]

Accordingly, in KI MV, we specifically detected the upregulation of a key enzyme involved in glycosaminoglycans production; the hyaluronan synthase 1 (*Has1*). In addition, the increased expression of metalloproteinases (*Mmp12*, *Mmp17*, *Adamts7*) as well as modulators (*Grem1*) or actors (*Tgfbr1*, *Smad4*) of key cytokines signaling pathways involved in valvular ECM remodeling highlight the interrelation between genes involved in ECM remodeling (i.e. MC2) and those related to the response to mechanical stress (i.e. MC5). Both transcriptomic and regulomic analyses point to specific activation of TGF-β and Wnt pathways in our model with also a role for the BMP pathway highlighted in the transcriptomic analysis.[10,31,34–36] This notion is consistent with the previously described crosstalk between mechanical stress and TGF-β signalings that participates in the establishment of this vicious circle which, in the context of MVD, leads to maintain the activation of MV valvular interstitial cells (VICs), and feeds the pathological degenerative process over time. This finding provides a pivotal molecular target related to the development of the MVD phenotype.

Epithelial cell migration (i.e. MC3) and processes related to EMT (i.e. MC4) were also highlighted in the RNA-seq analysis. Valvular endothelial cells (VECs) actively participate in valvulogenesis and MV homeostasis via their crosstalks with interstitial cells, and their functions and activities are known to be modulated by mechanical stress.[10,37–40] Accordingly to a central role of VEC in MVD, swollen VECs were more frequently observed in KI rats. Although controversy regarding the involvement of EMT in MVD persists in the litterature, our data suggest that the activation of EMT would be important in the pathophysiological processes, at least in the early stages of the disease.[10,37,41] Further studies are needed to confirm this finding.

Finally, we identified a transcriptomic and regulomic signature related to chemotaxis and leukocyte recruitment in MV from KI animals (MC1). Enrichment in bone marrow-derived cells, essentially macrophages, has been previously observed in mice and human MV.[31,42–44] These macrophages, including resident and recruited cells, are described to participate in valvulogenesis, in the maturation of the valve after birth and in the pathophysiological processes leading to myxomatous MV (i.e; FlnA-

MVD, syndromic MVD, drug-induced MVD, as well as model of myxomatous aortic valve disease).[17,31,42–46] All together, these data coupled with both our RNA-seq and ATAC-seq support a pivotal role of bone marrow-derived cells, and particularly macrophages, in MVD. The specific role of resident and/or recruited macrophages in MVD will require additionnal investigations.

All together, this study provides new hypotheses into the pathophysiological mechanisms involved in the early stages of mitral valve dystrophy with the interrelation of ECM regulation, mechanotransduction, immune cells, and potentially EMT processes (Figure 4). Protein-protein association networks, based on the RNA-seq and ATAC-seq analyses, depict a complex and interrelated crosstalk between cells (endothelial, interstitial and immune) and molecular signaling pathways involved in ECM homeostasis to promote MV tissue remodeling in MVD (Figure 6).

4.3 Limitations

The main limitation of this study is inherant to any animal study and refers to the translation of findings from animal model to human disease.[47] Notably, whereas structural remodeling differentially affecting anterior and posterior leaflets and functionnal MV disabilities (i.e. MVP, MV regurgitation and LV remodeling) depict MVD in patients, the FlnA-P637Q rat model analyzed until 6 months does not recapitulate the whole spectrum of these pathological traits. Both technical and conceptual limitations participate to this discrepency. For example, the poor spatial and temporal resolution of our echograph limited the quantitative assement of MV thickening, MV prolapse and mitral regurgitation. Also, even if we used fold-changes between littermate rats, the contrasting solution used for microCT scanning could result in differences between scans.

Transciptomic analyses also suffer from some limitations. The small number of replicates in RNA-seq limited the statistical power for this analysis. In addition, even if optimal sample quality to perform ATAC-seq analysis was indubitably reached and the findings corroborated RNA-seq analysis, the number of biological replicates used (n=2) remains small and interpretation should be done with caution. Moreover, biological material recovery (i.e. cells for ATAC-seq and RNA for RNA-seq and qPCR)

cannot be definitively assessed but we made sure that the digestion of tissue was completed and RNA recovery was proportional to the amount of tissue used. In any case, because RNA-seq analysis was performed on pooled anterior and posterior leaflets we could not detect gene expression differences between them. However, qPCR performed on key selected genes did not show significant differences between MV leaflets but, on the other hand, we cannot exclude that RNA-seq performed on separated anterior versus posterior leaflets would have identified potential differences in signaling pathways between them. Here again, the analysis of older animals and haemodynamically challenging conditions may alleviate these discrepencies. In this context, our study should be considered as hypothesis generating. However, the observed concordance in signaling pathways idenfied in both RNA-seq and ATAC-seq supports the robustness of our data and reinforces our findings. This metacluster-based analysis performed on a hypothesis-free approach could also mask pathways that will merit further attention: the response to mechanical stress, our central mechanistic hypothesis, was only highlighted by hypothesis-driven analysis but we could also consider an overlap with the MC2 “ECM remodeling”.

Finally, the aortic valve phenotype has not been evaluated and would require further investigations.

4.4 Conclusion

The KI FlnA-P637Q rat model mimics human myxomatous mitral valve dystrophy and opens new avenues to decipher molecular mechanisms associated with the development of this disease. We revealed that extracellular matrix organization, epithelial cells migration, response to mechanical stress, as well as a central contribution of immune cells response are important signaling pathways in the processes leading to MVD in both males and females. Our data pave the road to decipher underlying molecular mechanisms and the specific role of each cell sub-population in the development and progression of myxomatous mitral valve disease.

Funding: The present study has received funding from the European Union's Horizon 2020 research and innovation program under the Marie Sklodowska-Curie grant agreement No. 846291 and from the French Society of Cardiology under the "Alain Castaigne" scientific prize, both awarded to RC. RC is also supported by a "Connect Talent" research chair from Région Pays de la Loire and Nantes Métropole. Biogenouest and the Région Pays de la Loire supported the TRIP facility. EM and AHK are funded by the Deutsche Forschungsgemeinschaft (DFG, German Research Foundation) under Germany's Excellence Strategy – EXC2151 – 390873048. JB and AF are supported by the ANR JCJC LEARN (R21006NN, RPV21014NNA). MB is supported by IRP- VERACITIES - New Mechanisms for VEntricular ARrhythmia And CardIomeTabolic DIseasES, an I-SITE NExT health and engineering initiative (Ecole Centrale & Nantes University) and by the IRP- GAINES - Genetic Architecture IN cardiovascular disEaSes funded by INSERM and CNRS. PPG is supported by the ANR CROCOVAL (ANR-18-CE45-0015).

Acknowledgments: We acknowledge the IBISA MicroPICell facility (Biogenouest), a member of the national infrastructure France-Bioimaging supported by the French national research agency (ANR-10-INBS-04). We also acknowledge the Therassay, SC3M and the UTE facilities of the Structure Fédérative de Recherche François Bonamy (Nantes, France) for technical assistance. We thank Bastien Cimarosti for his precious help in R programming. We are grateful to the Genomics and Bioinformatics Core Facility of Nantes GenoBiRD, a member of Biogenouest, Institut Français de Bioinformatique (IFB) (ANR-11-INBS-0013) for the use of its resources and for its technical support.

Conflict of interest: The authors have reported no relationship relevant to the content of this paper to disclose.

REFERENCES

1. Nkomo VT, Gardin JM, Skelton TN, Gottdiener JS, Scott CG, Enriquez-Sarano M. Burden of valvular heart diseases: a population-based study. *The Lancet* 2006;**368**:1005–1011.

2. Baumgartner H, Falk V, Bax JJ, De Bonis M, Hamm C, Holm PJ, Iung B, Lancellotti P, Lansac E, Rodriguez Muñoz D, Rosenhek R, Sjögren J, Tornos Mas P, Vahanian A, Walther T, Wendler O, Windecker S, Zamorano JL, ESC Scientific Document Group. 2017 ESC/EACTS Guidelines for the management of valvular heart disease. *Eur Heart J* 2017;**38**:2739–2791.

3. Kyndt F, Schott J-J, Trochu J-N, Baranger F, Herbert O, Scott V, Fressinaud E, David A, Moisan J-P, Bouhour J-B, Le Marec H, Bénichou B. Mapping of X-Linked Myxomatous Valvular Dystrophy to Chromosome Xq28. *Am J Hum Genet* 1998;**62**:627–632.

4. Kyndt F, Gueffet J-P, Probst V, Jaafar P, Legendre A, Le Bouffant F, Toquet C, Roy E, McGregor L, Lynch SA, Newbury-Ecob R, Tran V, Young I, Trochu J-N, Le Marec H, Schott J-J. Mutations in the Gene Encoding Filamin A as a Cause for Familial Cardiac Valvular Dystrophy. *Circulation* 2007;**115**:40–49.

5. Durst R, Sauls K, Peal DS, deVlaming A, Toomer K, Leyne M, Salani M, Talkowski ME, Brand H, Perrocheau M, Simpson C, Jett C, Stone MR, Charles F, Chiang C, Lynch SN, Bouatia-Naji N, Delling FN, Freed LA, Tribouilloy C, Le Tourneau T, LeMarec H, Fernandez-Friera L, Solis J, Trujillano D, Ossowski S, Estivill X, Dina C, Bruneval P, Chester A, Schott J-J, Irvine KD, Mao Y, Wessels A, Motiwala T, Puceat M, Tsukasaki Y, Menick DR, Kasiganesan H, Nie X, Broome A-M, Williams K, Johnson A, Markwald RR, Jeunemaitre X, Hagege A, Levine RA, Milan DJ, Norris RA, Slaugenhaupt SA. Mutations in DCHS1 cause mitral valve prolapse. *Nature* 2015;**525**:109–113.

6. Toomer KA, Yu M, Fulmer D, Guo L, Moore KS, Moore R, Drayton KD, Glover J, Peterson N, Ramos-Ortiz S, Drohan A, Catching BJ, Stairley R, Wessels A, Lipschutz JH, Delling FN, Jeunemaitre X, Dina C, Collins RL, Brand H, Talkowski ME, Monte F del, Mukherjee R, Awgulewitsch A, Body S, Hardiman G, Hazard ES, Silveira WA da, Wang B, Leyne M, Durst R, Markwald RR, Le Scouarnec S, Hagege A, Le Tourneau T, Kohl P, Rog-Zielinska EA, Ellinor PT, Levine RA, Milan DJ, Schott J-J, Bouatia-Naji N, Slaugenhaupt SA, Norris RA. Primary cilia defects causing mitral valve prolapse. *Sci Transl Med* 2019;**11**:eaax0290.

7. Dina C, Bouatia-Naji N, Tucker N, Delling FN, Toomer K, Durst R, Perrocheau M, Fernandez-Friera L, Solis J, Le Tourneau T, Chen M-H, Probst V, Bosse Y, Pibarot P, Zelenika D, Lathrop M, Hercberg S, Roussel R, Benjamin EJ, Bonnet F, Lo SH, Dolmatova E, Simonet F, Lecointe S, Kyndt F, Redon R, Le Marec H, Froguel P, Ellinor PT, Vasan RS, Bruneval P, Markwald RR, Norris RA, Milan DJ, Slaugenhaupt SA, Levine RA, Schott J-J, Hagege AA, Jeunemaitre X, Schott J-J, Hagege AA, Jeunemaitre X. Genetic association analyses highlight biological pathways underlying mitral valve prolapse. *Nat Genet* 2015;**47**:1206–1211.

8. Yu M, Kyryachenko S, Debette S, Amouyel P, Schott J-J, Le Tourneau T, Dina C, Norris RA, Hagège AA, Jeunemaitre X, Bouatia-Naji N. Genome-Wide Association Meta-Analysis Supports Genes Involved in Valve and Cardiac Development to Associate With Mitral Valve Prolapse. *Circ Genomic Precis Med* 2021.

9. Roselli C, Yu M, Nauffal V, Georges A, Yang Q, Love K, Weng L-C, Delling FN, Maurya SR, Schrölkamp M, Tfelt-Hansen J, Hagège A, Jeunemaitre X, Debette S, Amouyel P, Guan W, Muehlschlegel JD, Body SC, Shah S, Samad Z, Kyryachenko S, Haynes C, Rienstra M, Le Tourneau T, Probst V, Roussel R, Wijdh-Den Hamer IJ, Siland JE, Knowlton KU, Jacques Schott J, Levine RA,

Benjamin EJ, Vasan RS, Horne BD, Muhlestein JB, Benfari G, Enriquez-Sarano M, Natale A, Mohanty S, Trivedi C, Shoemaker MB, Yoneda ZT, Wells QS, Baker MT, Farber-Eger E, Michelena HI, Lundby A, Norris RA, Slaugenhaupt SA, Dina C, Lubitz SA, Bouatia-Naji N, Ellinor PT, Milan DJ. Genome-wide association study reveals novel genetic loci: a new polygenic risk score for mitral valve prolapse. *Eur Heart J* 2022;**43**:1668–1680.

10. Levine RA, Hagége AA, Judge DP, Padala M, Dal-Bianco JP, Aikawa E, Beaudoin J, Bischoff J, Bouatia-Naji N, Bruneval P, Butcher JT, Carpentier A, Chaput M, Chester AH, Clusel C, Delling FN, Dietz HC, Dina C, Durst R, Fernandez-Friera L, Handschumacher MD, Jensen MO, Jeunemaitre XP, Marec HL, Tourneau TL, Markwald RR, Mérot J, Messas E, Milan DP, Neri T, Norris RA, Peal D, Perrocheau M, Probst V, Pucéat M, Rosenthal N, Solis J, Schott J-J, Schwammenthal E, Slaugenhaupt SA, Song J-K, Yacoub MH, Yacoub MH. Mitral valve disease—morphology and mechanisms. *Nat Rev Cardiol* 2015;**12**:689–710.

11. Le Tourneau T, Le Scouarnec S, Cueff C, Bernstein D, Aalberts JJJ, Lecointe S, Mérot J, Bernstein JA, Oomen T, Dina C, Karakachoff M, Desal H, Al Habash O, Delling FN, Capoulade R, Suurmeijer AJH, Milan D, Norris RA, Markwald R, Aikawa E, Slaugenhaupt SA, Jeunemaitre X, Hagège A, Roussel J-C, Trochu J-N, Levine RA, Kyndt F, Probst V, Le Marec H, Schott J-J. New insights into mitral valve dystrophy: a Filamin-A genotype–phenotype and outcome study. *Eur Heart J* 2018;**39**:1269–1277.

12. Bandaru S, Ala C, Zhou A-X, Akyürek LM. Filamin A Regulates Cardiovascular Remodeling. *Int J Mol Sci* 2021;**22**:6555.

13. Ketebo AA, Park C, Kim J, Jun M, Park S. Probing mechanobiological role of filamin A in migration and invasion of human U87 glioblastoma cells using submicron soft pillars. *Nano Converg* 2021;**8**:19.

14. Washington RW, Knecht DA. Actin binding domains direct actin-binding proteins to different cytoskeletal locations. *BMC Cell Biol* 2008;**9**:10.

15. Misra S, Ghatak S, Moreno-Rodriguez RA, Norris RA, Hascall VC, Markwald RR. Periostin/Filamin-A: A Candidate Central Regulatory Axis for Valve Fibrogenesis and Matrix Compaction. *Front Cell Dev Biol* 2021;**9**:649862.

16. Sauls K, Vlaming A de, Harris BS, Williams K, Wessels A, Levine RA, Slaugenhaupt SA, Goodwin RL, Pavone LM, Merot J, Schott J-J, Le Tourneau T, Dix T, Jesinkey S, Feng Y, Walsh C, Zhou B, Baldwin S, Markwald RR, Norris RA. Developmental basis for filamin-A-associated myxomatous mitral valve disease. *Cardiovasc Res* 2012;**96**:109–119.

17. Sauls K, Toomer K, Williams K, Johnson A, Markwald R, Hajdu Z, Norris R. Increased Infiltration of Extra-Cardiac Cells in Myxomatous Valve Disease. *J Cardiovasc Dev Dis* 2015;**2**:200–213.

18. Duval D, Lardeux A, Le Tourneau T, Norris RA, Markwald RR, Sauzeau V, Probst V, Le Marec H, Levine R, Schott JJ, Merot J. Valvular dystrophy associated filamin A mutations reveal a new role of its first repeats in small-GTPase regulation. *Biochim Biophys Acta BBA - Mol Cell Res* 2014;**1843**:234–244.

19. Duval D, Labbé P, Bureau L, Tourneau T, Norris R, Markwald R, Levine R, Schott J-J, Mérot J. MVP-Associated Filamin A Mutations Affect FlnA-PTPN12 (PTP-PEST) Interactions. *J Cardiovasc Dev Dis* 2015;**2**:233–247.

20. Haataja TJK, Bernardi RC, Lecointe S, Capoulade R, Merot J, Pentikäinen U. Non-syndromic Mitral Valve Dysplasia Mutation Changes the Force Resilience and Interaction of Human Filamin A. *Structure* 2019;**27**:102-112.e4.

21. Remy S, Chenouard V, Tesson L, Usal C, Ménoret S, Brusselle L, Heslan J-M, Nguyen TH, Bellien J, Merot J, De Cian A, Giovannangeli C, Concordet J-P, Anegon I. Generation of gene-edited rats by delivery of CRISPR/Cas9 protein and donor DNA into intact zygotes using electroporation. *Sci Rep* 2017;**7**:16554.

22. Chenouard V, Brusselle L, Heslan J-M, Remy S, Ménoret S, Usal C, Ouisse L-H, NGuyen TH, Anegon I, Tesson L. A Rapid and Cost-Effective Method for Genotyping Genome-Edited Animals: A Heteroduplex Mobility Assay Using Microfluidic Capillary Electrophoresis. *J Genet Genomics* 2016;**43**:341–348.

23. Love MI, Huber W, Anders S. Moderated estimation of fold change and dispersion for RNA-seq data with DESeq2. *Genome Biol* 2014;**15**:550.

24. Yu G, Wang L-G, Han Y, He Q-Y. clusterProfiler: an R Package for Comparing Biological Themes Among Gene Clusters. *OMICS J Integr Biol* 2012;**16**:284–287.

25. Robinson MD, McCarthy DJ, Smyth GK. edgeR: a Bioconductor package for differential expression analysis of digital gene expression data. *Bioinformatics* 2010;**26**:139–140.

26. Gise A von, Pu WT. Endocardial and Epicardial Epithelial to Mesenchymal Transitions in Heart Development and Disease. *Circ Res* 2012;**110**:1628–1645.

27. Feng Y, Chen MH, Moskowitz IP, Mendonza AM, Vidali L, Nakamura F, Kwiatkowski DJ, Walsh CA. Filamin A (FLNA) is required for cell-cell contact in vascular development and cardiac morphogenesis. *Proc Natl Acad Sci* 2006;**103**:19836–19841.

28. Oyama MA, Elliott C, Loughran KA, Kossar AP, Castillero E, Levy RJ, Ferrari G. Comparative pathology of human and canine myxomatous mitral valve degeneration: 5HT and TGF-β mechanisms. *Cardiovasc Pathol* 2020;**46**:107196.

29. Chenouard V, Remy S, Tesson L, Ménoret S, Ouisse L-H, Cherifi Y, Anegon I. Advances in Genome Editing and Application to the Generation of Genetically Modified Rat Models. *Front Genet* 2021;**12**:615491.

30. Rabkin E, Aikawa M, Stone JR, Fukumoto Y, Libby P, Schoen FJ. Activated Interstitial Myofibroblasts Express Catabolic Enzymes and Mediate Matrix Remodeling in Myxomatous Heart Valves. *Circulation* 2001;**104**:2525–2532.

31. Geirsson A, Singh M, Ali R, Abbas H, Li W, Sanchez JA, Hashim S, Tellides G. Modulation of Transforming Growth Factor- Signaling and Extracellular Matrix Production in Myxomatous Mitral Valves by Angiotensin II Receptor Blockers. *Circulation* 2012;**126**:S189–S197.

32. Dal-Bianco JP, Aikawa E, Bischoff J, Guerrero JL, Hjortnaes J, Beaudoin J, Szymanski C, Bartko PE, Seybolt MM, Handschumacher MD, Sullivan S, Garcia ML, Mauskapf A, Titus JS, Wylie-Sears J, Irvin WS, Chaput M, Messas E, Hagège AA, Carpentier A, Levine RA. Myocardial Infarction Alters Adaptation of the Tethered Mitral Valve. *J Am Coll Cardiol* 2016;**67**:275–287.

33. Marsit O, Clavel M-A, Côté-Laroche C, Hadjadj S, Bouchard M-A, Handschumacher MD, Clisson M, Drolet M-C, Boulanger M-C, Kim D-H, Guerrero JL, Bartko PE, Couet J, Arsenault M, Mathieu

P, Pibarot P, Aïkawa E, Bischoff J, Levine RA, Beaudoin J. Attenuated Mitral Leaflet Enlargement Contributes to Functional Mitral Regurgitation After Myocardial Infarction. *J Am Coll Cardiol* 2020;**75**:395–405.

34. Neptune ER, Frischmeyer PA, Arking DE, Myers L, Bunton TE, Gayraud B, Ramirez F, Sakai LY, Dietz HC. Dysregulation of TGF-β activation contributes to pathogenesis in Marfan syndrome. *Nat Genet* 2003;**33**:407–411.

35. Ng CM, Cheng A, Myers LA, Martinez-Murillo F, Jie C, Bedja D, Gabrielson KL, Hausladen JMW, Mecham RP, Judge DP, Dietz HC. TGF-β–dependent pathogenesis of mitral valve prolapse in a mouse model of Marfan syndrome. *J Clin Invest* 2004;**114**:1586–1592.

36. Schroer AK, Merryman WD. Mechanobiology of myofibroblast adhesion in fibrotic cardiac disease. *J Cell Sci* 2015;**128**:1865–1875.

37. Armstrong EJ, Bischoff J. Heart Valve Development: Endothelial Cell Signaling and Differentiation. *Circ Res* 2004;**95**:459–470.

38. Gee TW, Richards JM, Mahmut A, Butcher JT. Valve endothelial-interstitial interactions drive emergent complex calcific lesion formation in vitro. *Biomaterials* 2021;**269**:120669.

39. Hulin A, Hortells L, Gomez-Stallons MV, O'Donnell A, Chetal K, Adam M, Lancellotti P, Oury C, Potter SS, Salomonis N, Yutzey KE. Maturation of heart valve cell populations during postnatal remodeling. *Development* 2019;**146**:dev173047.

40. Butcher JT, Nerem RM. Valvular endothelial cells regulate the phenotype of interstitial cells in co-culture: effects of steady shear stress. *Tissue Eng* 2006;**12**:905–915.

41. Kim AJ, Alfieri CM, Yutzey KE. Endothelial Cell Lineage Analysis Does Not Provide Evidence for EMT in Adult Valve Homeostasis and Disease. *Anat Rec* 2019;**302**:125–135.

42. Hulin A, Anstine LJ, Kim AJ, Potter SJ, DeFalco T, Lincoln J, Yutzey KE. Macrophage transitions in heart valve development and myxomatous valve disease. *Arterioscler Thromb Vasc Biol* 2018;**38**:636–644.

43. Visconti RP, Ebihara Y, LaRue AC, Fleming PA, McQuinn TC, Masuya M, Minamiguchi H, Markwald RR, Ogawa M, Drake CJ. An In Vivo Analysis of Hematopoietic Stem Cell Potential: Hematopoietic Origin of Cardiac Valve Interstitial Cells. *Circ Res* 2006;**98**:690–696.

44. Hajdu Z, Romeo SJ, Fleming PA, Markwald RR, Visconti RP, Drake CJ. Recruitment of bone marrow-derived valve interstitial cells is a normal homeostatic process. *J Mol Cell Cardiol* 2011;**51**:955–965.

45. Hulin A, Moore V, James JM, Yutzey KE. Loss of Axin2 results in impaired heart valve maturation and subsequent myxomatous valve disease. *Cardiovasc Res* 2017;**113**:40–51.

46. Kim AJ, Xu N, Umeyama K, Hulin A, Ponny SR, Vagnozzi RJ, Green EA, Hanson P, McManus BM, Nagashima H, Yutzey KE. Deficiency of Circulating Monocytes Ameliorates the Progression of Myxomatous Valve Degeneration in Marfan Syndrome. *Circulation* 2020;**141**:132–146.

47. Leenaars CHC, Kouwenaar C, Stafleu FR, Bleich A, Ritskes-Hoitinga M, De Vries RBM, Meijboom FLB. Animal to human translation: a systematic scoping review of reported concordance rates. *J Transl Med* 2019;**17**:223.

FIGURE LEGENDS

FIGURE 1: Echocardiographic assessment of the mitral valve in 3-week-old KI FlnA-P637Q rats.

Legend: Mitral valve apparatus has been assessed by qualitative and quantitative approaches in 3-week-old WT and KI rats. Panel A shows the anterior MV leaflet in the open position: we observed a restrictive motion of the leaflet in diastole and measured the leaflet's length (white arrow). Panel B shows anterior and posterior MV leaflets in the closed position, where MV prolapse is visualized (dash line: annulus plan; red arrow: prolapse of the posterior leaflet). Anterior leaflet length (Panel C), annulus diameter (Panel D), and heart rate (Panel E) were compared between KI and WT rats. All the analyses (Panels C to E) were performed on 5 WT and 10 KI littermate rats (all as biological replicates). P-values are from the Mann-Whitney test. Error bars represent the standard error of the mean (SEM). LA: left atrium; LV left ventricle; ns: not significant.

FIGURE 2: 3D mitral valve volume assessed by micro-computed tomography.

Legend: Panels A to F describe the protocol for MV volume quantification. Panel A shows the reconstructed full heart. 3-plan full heart views were used to crop the region of interest containing the mitral valve (Panel B). Panel C shows the cropped 2D view from panel B focused on the mitral valve. Manual segmentation of the mitral valve on 2D images is presented in Panel D. Otsu 3-level thresholding method is applied to the valve (Panel E) allowing us to get a 3D reconstructed volume of the valve (atrial view, Panel F). Panel G represents the increase in microCT-derived MV volume defined as the fold-change between KI and WT littermate animals; these fold-changes were calculated for 11 KI animals (all as biological replicates). The ventricular view of the representative 3D reconstruction of MV from WT and KI rats is presented in Panel H. P-value is from the Wilcoxon test. Error bar represents the standard error of the mean (SEM). Ant: Anterior Leaflet; Post: Posterior Leaflet.

FIGURE 3: Macroscopic remodeling and histological evaluation of WT and KI mitral valves.

Legend: Panel A presents captions of the macroscopic aspect of the MV, highlighting the thickened (opaque) areas on the KI anterior and posterior leaflets. Note the thickened and less branched nature of the MV chordae (black arrowheads) in KI rats. Panel A' refers to the number of branches of chordae tendinae in KI animals compared to WT (n=11 WT *versus* n=12 KI). Standard Hematoxylin Phloxin Eosin (Panels B,E,H,I), Alcian Blue (Panels C,F,J,K) and Masson's trichrome (Panels D,G,L,M) histological stainings performed in consecutive slides on the MV of WT (Panels B-D and H,J,L) and KI (Panels E-G and I,K,M) rats. Panels H to M are area magnifications of the posterior leaflets. WT rats presented thin leaflets (Panels B,H) with very few proteoglycans (Panels C,J) and dense collagen strips (Panels D,L). KI rats presented an accumulation of proteoglycans (Panels F,K) and disrupted collagen (Panels G,M). These images are representatives of the cohort of 5 WT and 10 KI rats (all as biological replicates). Panels N and O present the quantitative analysis of the thickness and the alcian blue signal respectively, for each third of the leafet (i.e. normalized by the length of the leaflet) and presented as a fold change for each KI versus its WT littermate (n=5 WT and n=10 KI). White scale bars=2mm for Panels A and A'. Black scale bars= 250µm for Panels B to G. Black scale bars= 50µm for Panels H to M. *: $p<0.05$ from WT. ns: non-significant p-value from WT. P-values are from the Wilcoxon test or Mann-Whitney test, as appropriate. Error bar represents the standard error of the mean (SEM).

FIGURE 4: Molecular phenotyping for the identification of signaling pathways related to MVD.

Legend: Transcriptomic analysis of WT *versus* KI mitral valves. Panel A represents a heatmap of the 524 differentially expressed genes (i.e. as defined by $p<0.05$ and FC>1.2 or FC<0.8) highlighting genotype clusterization. Panel B shows the metaclusters analysis. Heatmaps on the left present normalized expression values for individual genes according to biological conditions on a normalized scale (from -1 to 1). The 5 metaclusters (MC1-5) were created based on the biological process of a GO enrichment analysis. Metaclusters represent groups of genes associated with similar biological functions and

corresponding GO-terms are listed in the second column. All the differentially expressed genes for each metacluster are listed on the right (upregulated genes are in bold). The analysis was performed on 5 WT and 4 KI mitral valves (all as biological replicates).

FIGURE 5: Chromatin opening analysis by ATAC-seq between KI and WT conditions.

Legend: ATAC-seq has been performed on WT and KI mitral valve cells from 3-week-old rats. The volcano plot (Panel A) shows the 21 significant transcription factors with a differential transcription factors binding dynamic. Significant transcription factors with differential binding dynamic (defined with the threshold > abs(0.09) and log10(p-value) > 100) are depicted in red when a transcription factor foot-printing is over-represented in KI than in WT and in blue for the opposite. Aggregated footprints between bound sites are shown for FOSL1 and JUND, two of the most differentially binding transcription factors between KI and WT. Panel B shows the Enrichr enrichment analysis tool results using the Panther DB 2016 and WikiPathway 2021 with a log10 corrected p-value (Bonferroni). Panel C (UCSC browser screenshot) represents example regions for four genes found both in differentially opened regions between KI and WT and genes identified in the MC analysis. Differentially opened regions (peaks) are indicated with a red asterisk. Footprinting of the 21 transcription factors identified by TOBIAS is indicated in green when overlapping a differentially opened region. The analysis was performed on 2 samples of 50 000 cells from WT and KI mitral valves (all as biological replicates).

FIGURE 6: Protein-protein association network based on selected genes associated with MVD.

Legend: Representation of the crosstalk between valvular cells (i.e. endothelial, interstitial and immune cells) and signaling actors of ECM homeostasis. Known and predicted functional and physical protein associations of the most relevant genes associated with MV tissue remodeling identified in both RNA-seq and ATAC-seq analysis (Table; Figure 5; Online supplemental Table S4) using STRING database are presented. Active interaction sources are textmining, experiments, databases, co-

expression, neighborhood, gene fusion and co-occurrence. Line thickness indicates the strength of data support.

TABLE: Relevant differentially expressed genes from metaclusters transcriptomic analysis

Gene	FC	p-value
Chemotaxis and immune cell migration		
Ccl28	1.53	0.047
Ccl7	2.95	4.76E-07
Il16	1.25	2.81E-03
Itgax	1.73	0.010
Itga9	0.78	0.023
Madcam1	5.70	0.039
S100a8	8.40	5.12E-03
S100a9	2.67	0.015
Extracellular matrix		
Adamts7	1.22	9.69E-03
Has1	3.04	3.37E-09
Mmp12	2.44	6.38E-07
Mmp17	1.68	0.013
Epithelial cell migration		
Hbegf	1.48	0.013
Hyal1	0.70	0.020
Klf4	1.31	1.62E-03
Endothelial to mesenchymal transition		
Mef2c	1.34	4.92E-03
Tmem100	1.39	1.17E-03
Wnt2	0.71	0.023
Molecular stress pathways		
Bmp7	0.69	0.035
Cspg4	1.27	3.72E-03
Fosl1	3.40	1.79E-04
Grem1	2.87	3.41E-03
Htr2a	2.17	9.65E-03
Jund	0.85	0.055
Robo2	1.75	6.04E-04
Slit2	1.24	0.015
Smad4	1.25	0.036
Smoc2	0.37	0.026
Tgfbr1	1.21	0.038
Tll2	10.36	0.019
Vegfd	0.70	0.035

Legend: Fold Change (FC) and p-value of each differentially expressed gene presented in the metacluster analysis.

FIGURE 1

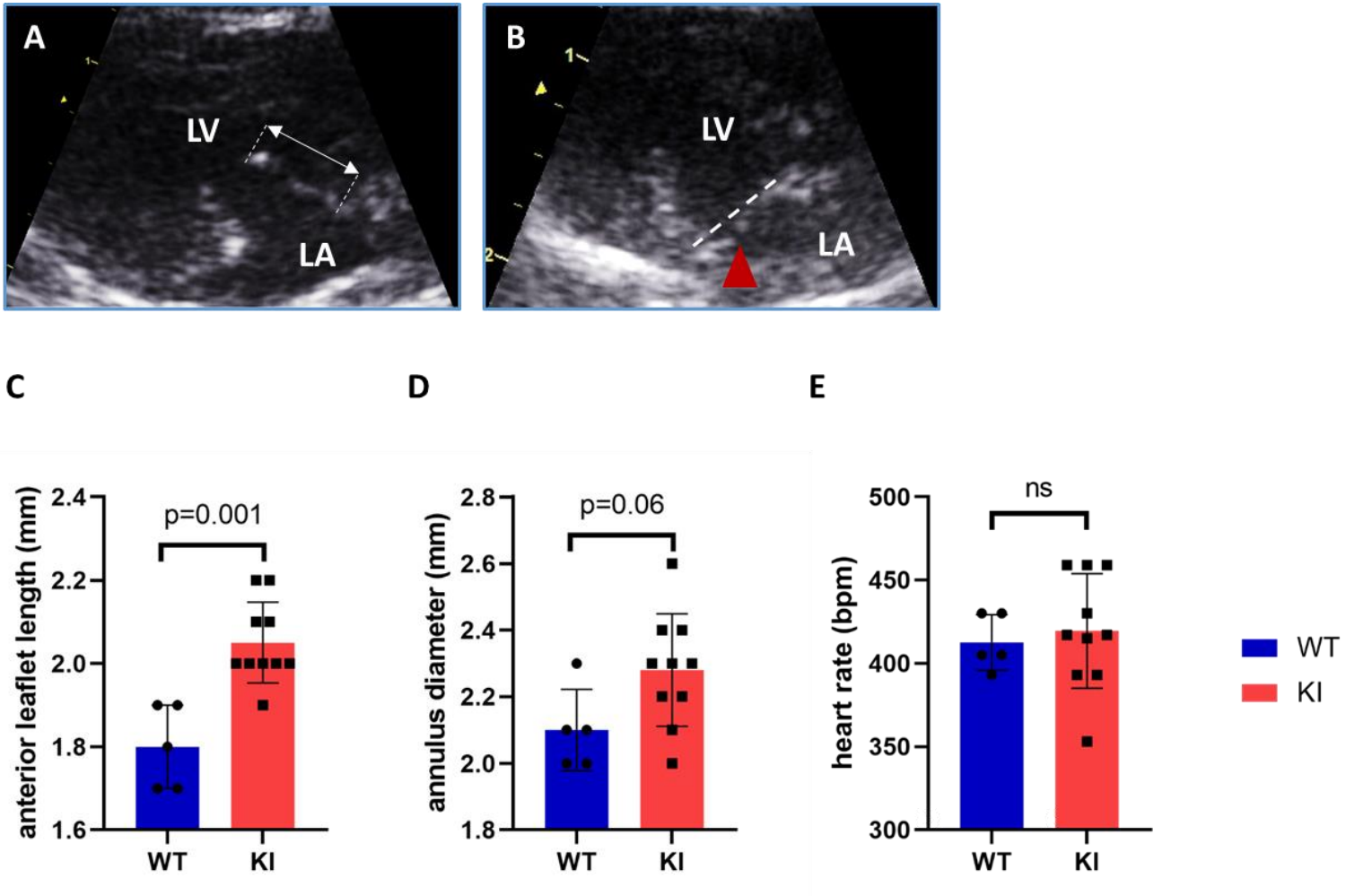
A
LV
LA
B
LV
LA
C
D
E
anterior leaflet length (mm)
2.4
2.2
2.0
1.8
1.6
p=0.001
WT
KI
annulus diameter (mm)
2.8
2.6
2.4
2.2
2.0
1.8
p=0.06
WT
KI
heart rate (bpm)
500
450
400
350
300
ns
WT
KI
WT
KI

FIGURE 2

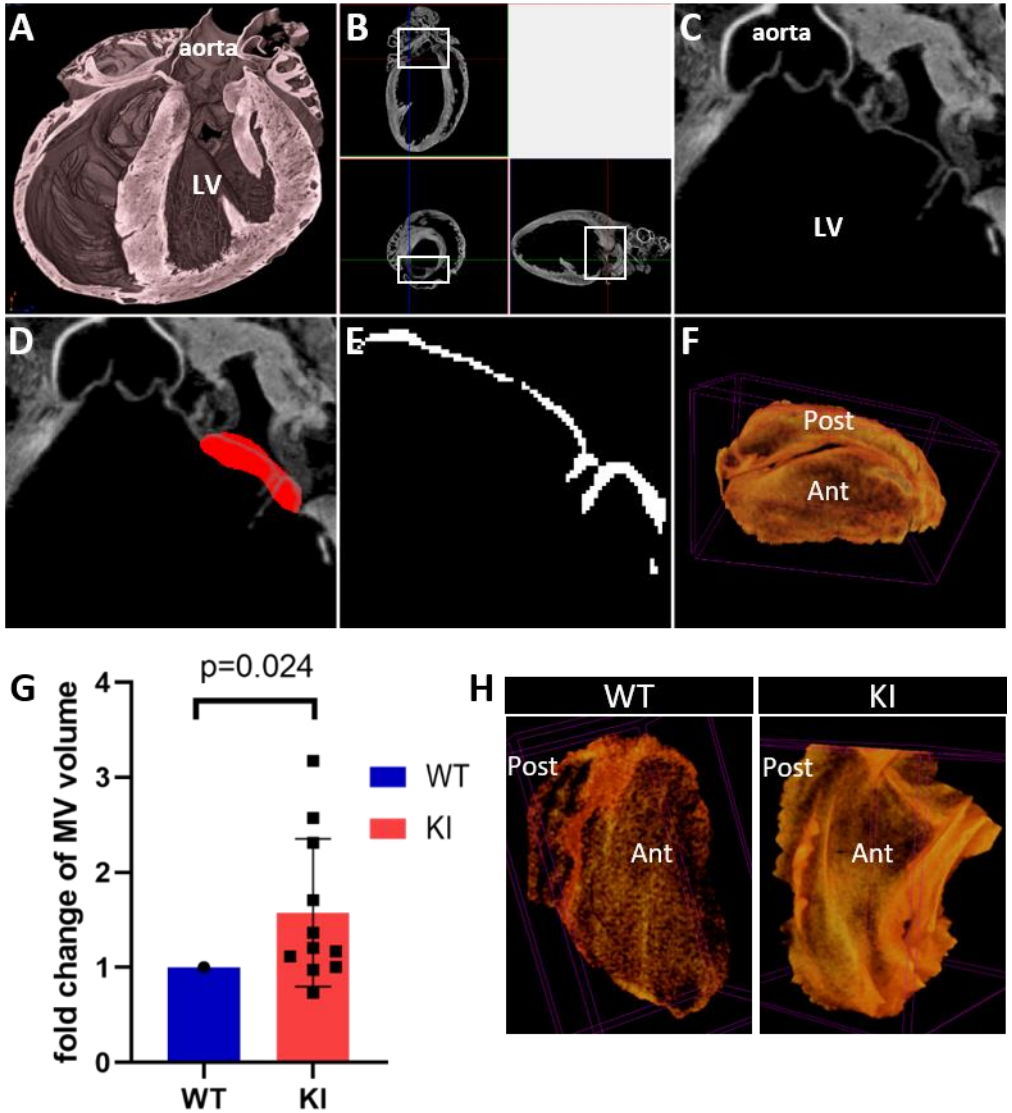
A
aorta
LV
B
C
aorta
LV
D
E
F
Post
Ant
G
p=0.024
fold change of MV volume
4
3
2
1
0
WT
KI
WT
KI
H
WT
KI
Post
Ant
Post
Ant

FIGURE 3

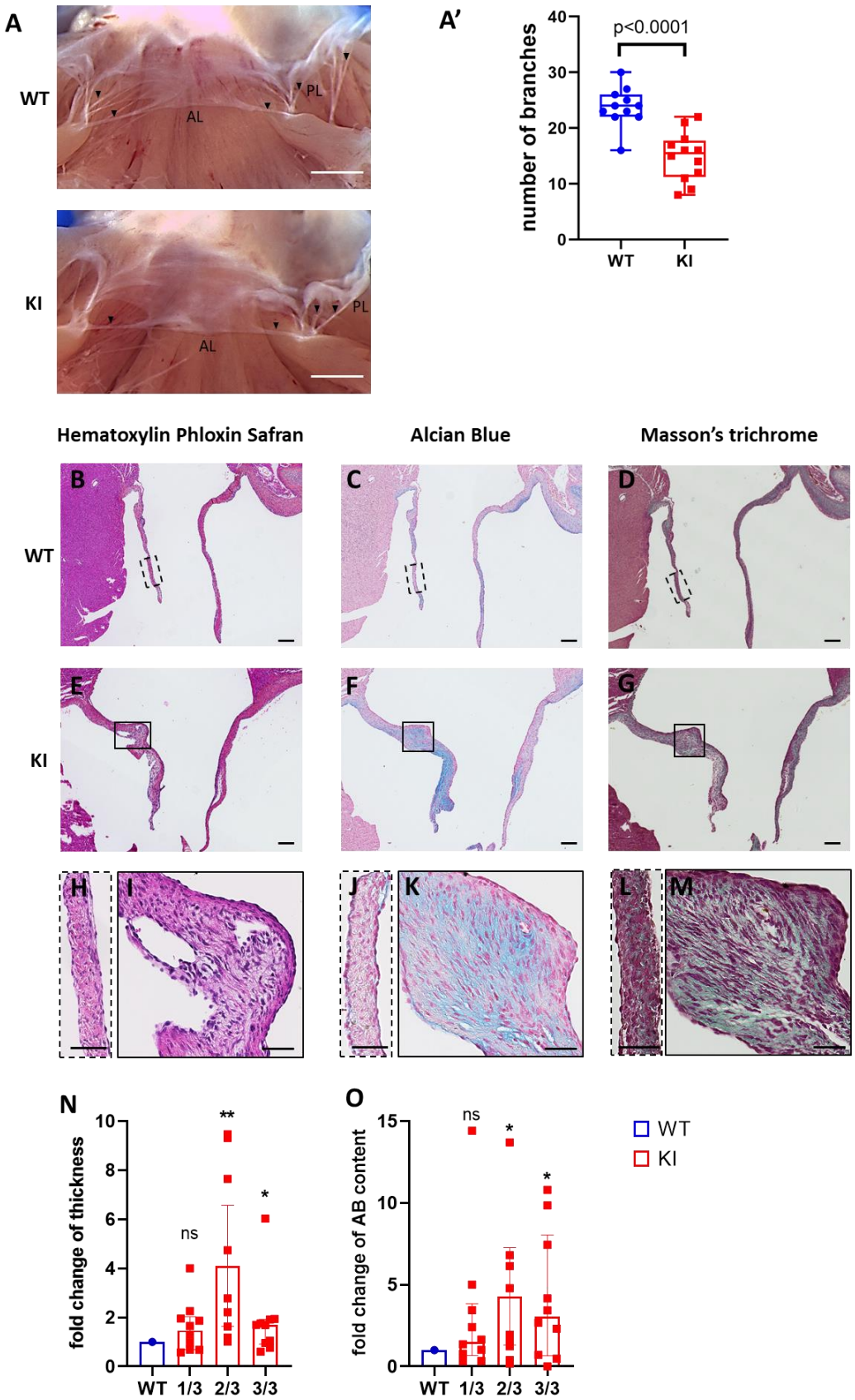
A
WT
KI
AL
PL
A'
number of branches
p<0.0001
WT
KI
Hematoxylin Phloxin Safran
Alcian Blue
Masson's trichrome
B
C
D
E
F
G
H
I
J
K
L
M
N
fold change of thickness
ns
**
*
WT 1/3 2/3 3/3
O
fold change of AB content
ns
*
*
WT 1/3 2/3 3/3
WT
KI

FIGURE 4

A

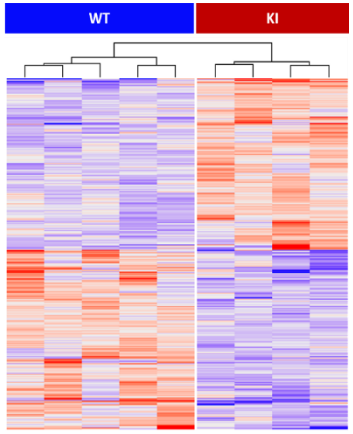

B

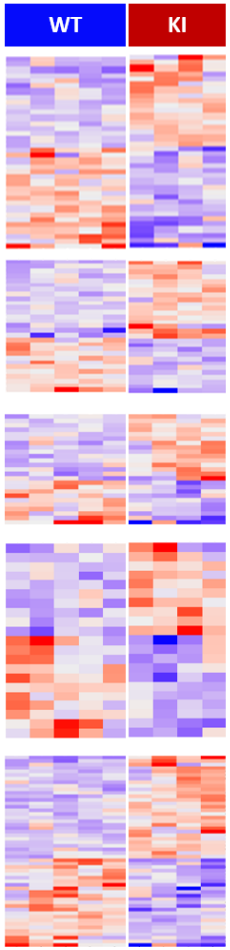

Normalized expression

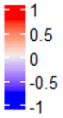

Metaclusters	GO-terms	Genes
MC1 Chemotaxis and immune cell migration	regulation of chemotaxis cell chemotaxis positive chemotaxis leukocyte chemotaxis regulation of positive chemotaxis neutrophil chemotaxis leukocyte migration neutrophil migration positive regulation of lymphocyte migration	***Angpt1***, ***Angpt2***, *Angpt4*, ***Ccl28***, *Ccl5*, ***Ccl7***, ***Cdh13***, *Cd2*, *Cx3cl1*, *Cxcl12*, *Cxcl13*, *Cxcl14*, *Cxcr4*, *Cxcr5*, ***Dock8***, ***Dok2***, *Dpp4*, ***Epha2***, *Fut7*, *F3*, ***Gpnmb***, ***Grem1***, ***Hbegf***, ***Il16***, *Itga9*, ***Itgax***, ***Itgb2***, ***Lpar1***, ***Madcam1***, *Ntrk3*, ***Olr1***, *Pla2g1b*, *Prex1*, *Rarres2*, ***Robo2***, ***S100a8***, ***S100a9***, *Sema3b*, *Sema3d*, ***Sema3e***, *Sema5b*, ***Slit2***, *Smoc2*, *Vegfd*
MC2 Extracellular Matrix	extracellular matrix organization extracellular structure organization	***Adamts7***, *Col18a1*, *Col22a1*, *Col9a3*, *Ddr1*, *Dpp4*, ***Egfl6***, *Egflam*, ***Ero1a***, *Fgfr4*, ***Grem1***, ***Has1***, *Itga9*, ***Itgax***, ***Itgb2***, ***Itgb6***, ***Kazald1***, ***Lama1***, ***Lcp1***, ***Madcam1***, ***Mmp12***, ***Mmp17***, *Ntng2*, ***Rgcc***, *Serac1*, *Sfrp2*, *Smoc2*, ***Tgfbr1***, ***Tll2***
MC3 Epithelial cell migration	epithelial cell migration epithelium migration	***Angpt1***, ***Angpt2***, *Angpt4*, *Apoe*, ***Cdh13***, *Cxcl13*, *Dpp4*, *Enpp2*, ***Epha2***, *Glipr2*, ***Grem1***, ***Hbegf***, *Hyal1*, ***Itgb2***, ***Klf4***, ***Mef2c***, ***Plcg2***, ***Prkx***, *Prox1*, *Ptgs2*, ***Rgcc***, ***Sirt1***, ***Slit2***, *Smoc2*, ***Tgfbr1***
MC4 Endothelial to mesenchymal transition	epithelial to mesenchymal transition cardiac epithelial to mesenchymal transition positive regulation of epithelial to mesenchymal transition cell migration involved in heart development negative regulation of epithelial cell proliferation regulation of cardiac epithelial to mesenchymal transition positive regulation of endothelial cell differentiation endothelial cell development	*Apoe*, *Bmp7*, *Cebpd*, *Cldn1*, *Col18a1*, ***Ezr***, *Flrt3*, ***Fst***, *Fuz*, *Glipr2*, ***Grem1***, ***Gsk3b***, ***Mef2c***, *Psmb9*, ***Rgcc***, *Sfrp2*, ***Sfrp4***, ***Smad4***, ***Tgfbr1***, ***Tmem100***, *Wnt2*
MC5 Molecular stress pathways	response to mechanical stimulus response to laminar fluid shear stress response to muscle stretch regulation of MAPK cascade regulation of stress activated protein kinase signaling cascade regulation of cellular response to growth factor stimulus smad protein signal transduction stress activated protein kinase signaling cascade	***Angpt1***, ***Angpt2***, *Apoe*, ***Avpi1***, *Bmp7*, ***Ccl7***, *Chi3l1*, *Cilp*, ***Cspg4***, ***Ctdspl2***, *Cx3cl1*, *Cxcl13*, *Cxcl12*, *Cxcr4*, ***Epha2***, ***Errfi1***, ***Etv1***, ***Ezr***, *Fgf9*, *Fgfr4*, ***Fosl1***, ***Fst***, *Fuz*, ***Gdf11***, *Glipr2*, ***Gpnmb***, ***Grem1***, ***Htr2a***, *Igfbp4*, *Il1rap*, ***Klf4***, *Lmo3*, ***Lpar1***, *Mapk11*, ***Mapk13***, ***Mapkapk3***, ***Mst1r***, *Ntrk3*, *Pak3*, *Pla2g1b*, *Ptgs2*, *Ret*, *Rgs2*, *Sfrp2*, ***Sfrp4***, *Shisa2*, ***Sirt1***, ***Slit2***, ***Smad4***, *Smoc2*, ***Tgfbr1***

FIGURE 5

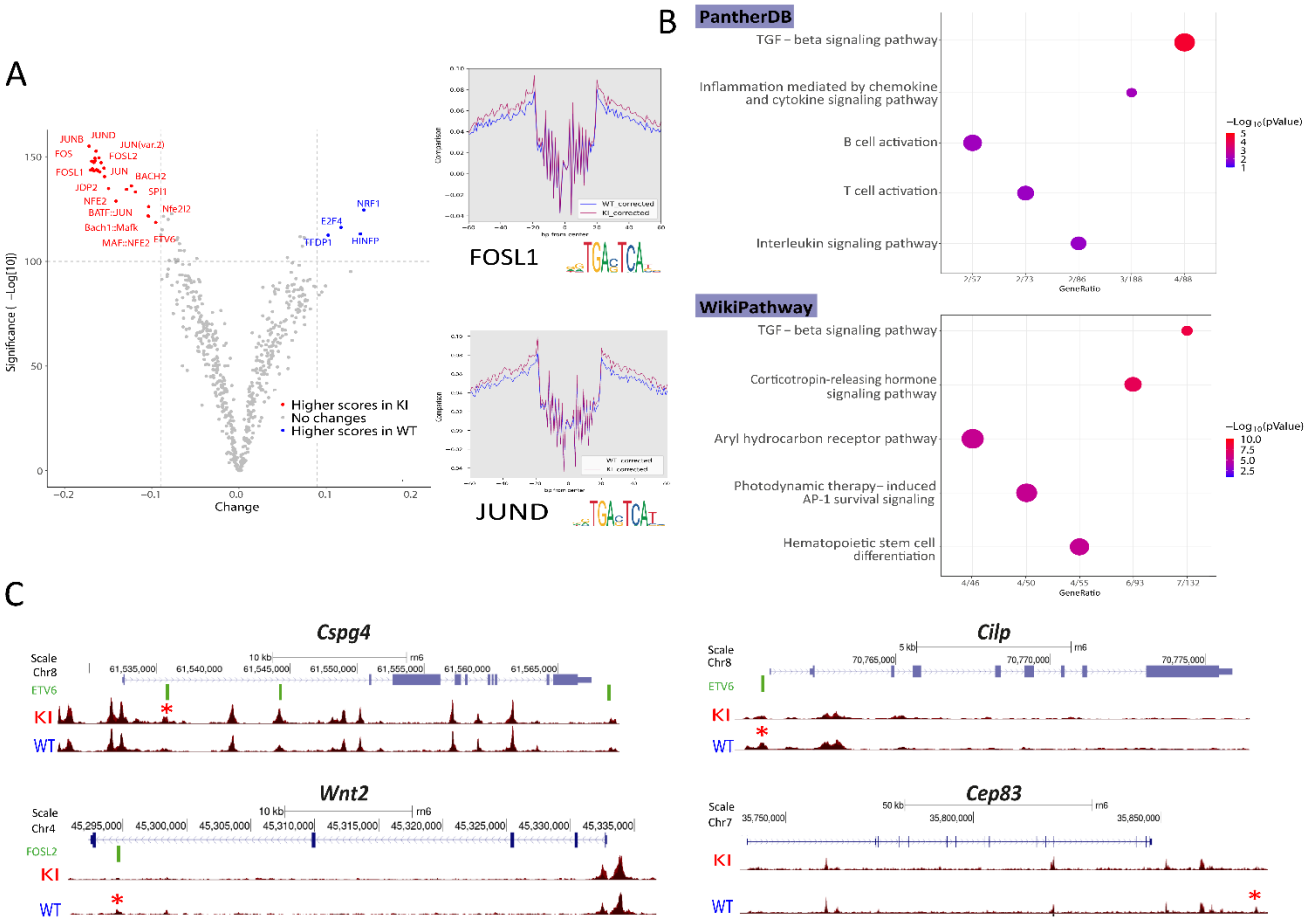
A
B
PantherDB
TGF – beta signaling pathway
Inflammation mediated by chemokine and cytokine signaling pathway
B cell activation
T cell activation
Interleukin signaling pathway
GeneRatio
−Log10(pValue)
WikiPathway
TGF – beta signaling pathway
Corticotropin-releasing hormone signaling pathway
Aryl hydrocarbon receptor pathway
Photodynamic therapy– induced AP-1 survival signaling
Hematopoietic stem cell differentiation
Significance (−Log10)
Change
Higher scores in KI
No changes
Higher scores in WT
FOSL1
JUND
C
Cspg4
Wnt2
Cilp
Cep83
Scale
Chr8
Chr4
Chr7
ETV6
FOSL2
KI
WT

FIGURE 6

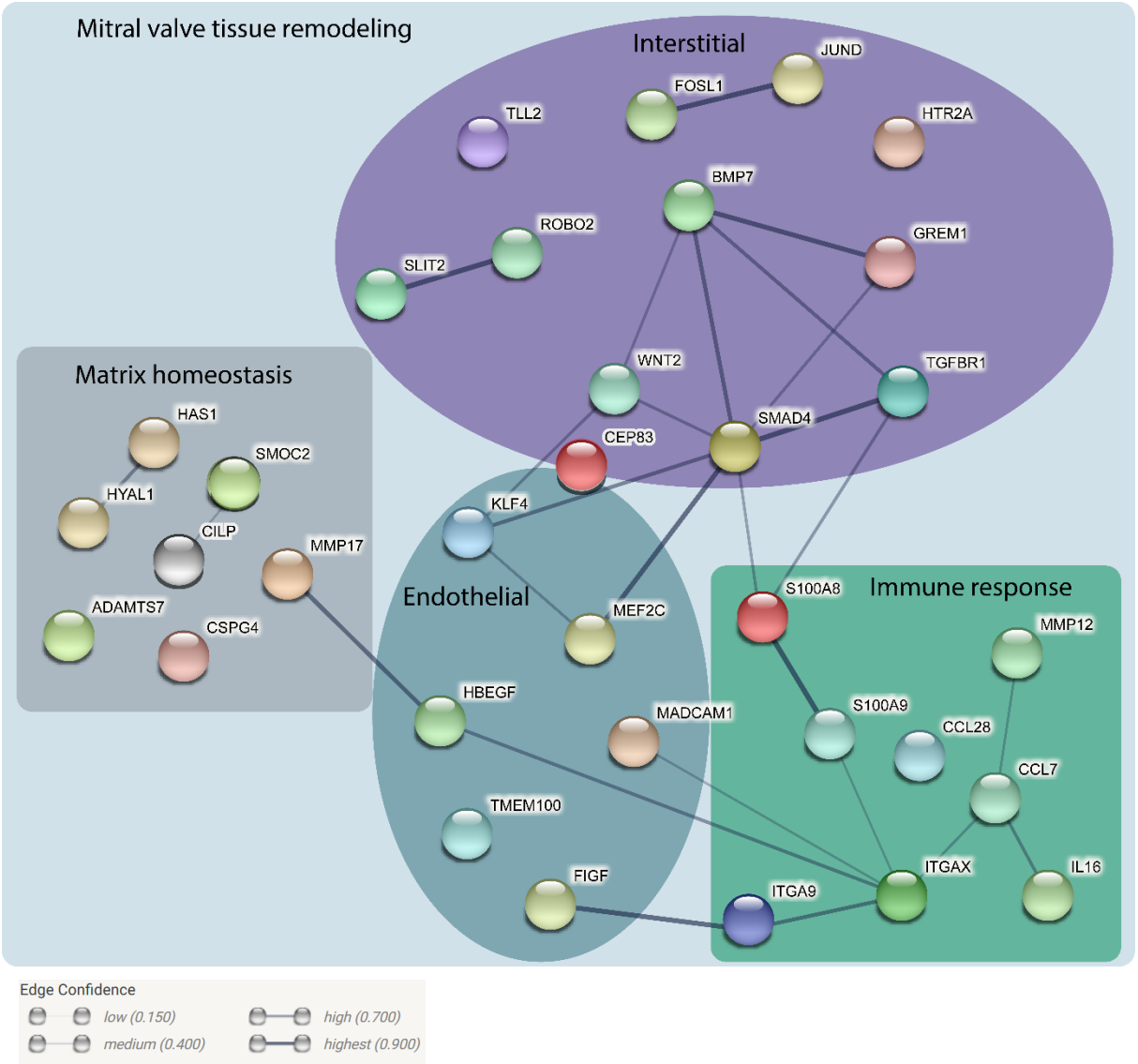
Mitral valve tissue remodeling
Interstitial
JUND
FOSL1
TLL2
HTR2A
BMP7
ROBO2
GREM1
SLIT2
WNT2
TGFBR1
SMAD4
CEP83
Matrix homeostasis
HAS1
SMOC2
HYAL1
CILP
MMP17
ADAMTS7
CSPG4
KLF4
Endothelial
MEF2C
HBEGF
MADCAM1
TMEM100
FIGF
S100A8
Immune response
MMP12
S100A9
CCL28
CCL7
ITGAX
IL16
ITGA9
Edge Confidence
low (0.150)
medium (0.400)
high (0.700)
highest (0.900)